Obesity remodels activity and transcriptional state of a lateral hypothalamic brake on feeding

Mark A. Rossi[1]*†, Marcus L. Basiri[1]*†, Jenna A. McHenry[1], Oksana Kosyk[1], James M. Otis[1], Hanna E. van den Munkhof[1], Julien Bryois[2], Christopher Hübel[2,3,4], Gerome Breen[3,4], Wilson Guo[1], Cynthia M. Bulik[1,2,5], Patrick F. Sullivan[2,6], Garret D. Stuber[1,7,8]†‡

The current obesity epidemic is a major worldwide health concern. Despite the consensus that the brain regulates energy homeostasis, the neural adaptations governing obesity are unknown. Using a combination of high-throughput single-cell RNA sequencing and longitudinal in vivo two-photon calcium imaging, we surveyed functional alterations of the lateral hypothalamic area (LHA)—a highly conserved brain region that orchestrates feeding—in a mouse model of obesity. The transcriptional profile of LHA glutamatergic neurons was affected by obesity, exhibiting changes indicative of altered neuronal activity. Encoding properties of individual LHA glutamatergic neurons were then tracked throughout obesity, revealing greatly attenuated reward responses. These data demonstrate how diet disrupts the function of an endogenous feeding suppression system to promote overeating and obesity.

Obesity affects more than 500 million adults worldwide (*1*), and its comorbidities present a pressing medical challenge (*2*). Within the brain, the lateral hypothalamic area (LHA) mediates motivated behavior, including feeding (*3–6*). LHA lesions abolish feeding and alter body weight regulation (*7*), whereas local electrical stimulation promotes ingestion and is rewarding (*3*). The LHA is molecularly and functionally diverse, comprising numerous cell types that can independently regulate food intake (*8–11*). We aimed to understand how obesity affects particular cells within the LHA.

We transcriptionally profiled LHA cells in lean and obese mice maintained on a control diet or a high-fat diet (HFD), respectively, using high-throughput single-cell RNA sequencing (Fig. 1, A and B, and fig. S1) (*12*). To detect discrete cell classes, cells were clustered on principal components and visualized via t-stochastic neighbor embedding (tSNE) for subsequent feature discovery (*13*). We identified transcriptionally distinct neuronal, glial, and stromal cell classes based on canonical marker distribution (Fig. 1, C to E). Cellular identities and proportions were similar between the sequencing and fluorescence in situ hybridization results (Fig. 1F and figs. S2 and S3), confirming the biological validity of statistical clustering.

We compared differential gene expression between HFD and control animals within each cluster and observed distinct patterns of transcriptional modification to the HFD across each

[1]Department of Psychiatry, University of North Carolina, Chapel Hill, NC 27599, USA. [2]Department of Medical Epidemiology and Biostatistics, Karolinska Institutet, Stockholm, Sweden. [3]Social, Genetic & Developmental Psychiatry Centre, Institute of Psychiatry, Psychology & Neuroscience, King's College London, UK. [4]UK National Institute for Health Research Biomedical Research Centre at South London and Maudsley Hospital, London, UK. [5]Department of Nutrition, University of North Carolina, Chapel Hill, NC 27599, USA. [6]Department of Genetics, University of North Carolina, Chapel Hill, NC 27599, USA. [7]Neuroscience Center, University of North Carolina at Chapel Hill, Chapel Hill, NC 27599, USA. [8]Department of Cell Biology and Physiology, University of North Carolina at Chapel Hill, Chapel Hill, NC 27599, USA.
*These authors contributed equally to this work. †Present address: Department of Anesthesiology and Pain Medicine, Department of Pharmacology, The Center for the Neurobiology of Addiction, Pain, and Emotion, University of Washington, Seattle, WA 98199, USA.
‡Corresponding author. Email: gstuber@uw.edu

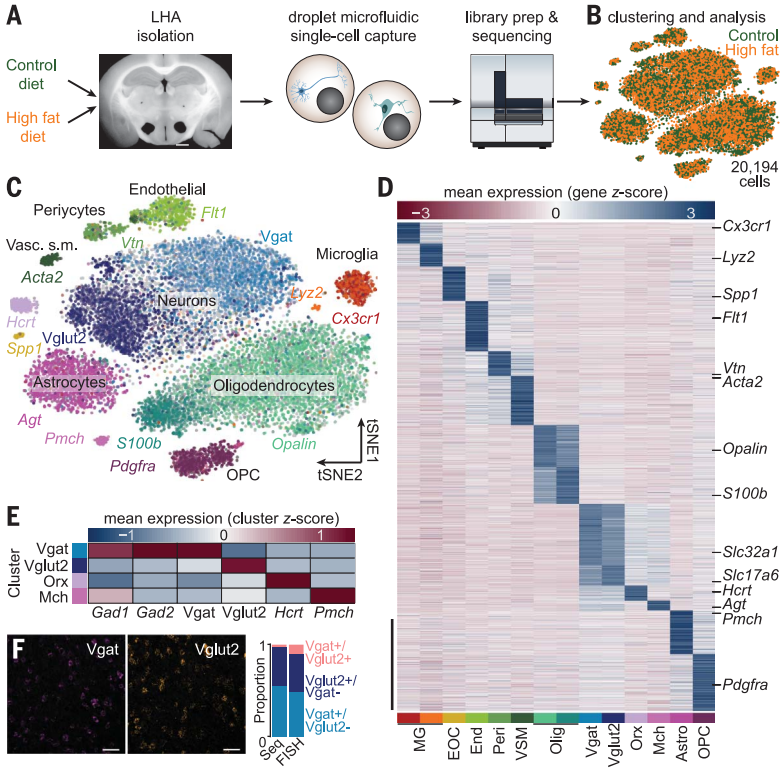

Fig. 1. Transcriptional profiling of LHA cells after chronic HFD exposure. (**A**) Schematic of experimental pipeline (n = 7 control mice, 10,086 cells; n = 7 HFD mice, 10,108 cells). Scale bar, 1 mm. (**B**) tSNE visualization of 20,194 cells. Control and HFD cells were clustered together. (**C**) tSNE visualization of 14 transcriptionally distinct clusters expressing canonical markers. (**D**) Statistically defined clusters exhibit distinct expression patterns. Scale bar, 500 genes. (**E**) Four clusters represent known LHA neuronal populations. (**F**) Fluorescence in situ hybridization (FISH) results. Scale bar, 50 μm. The proportion of cells expressing Vgat, Vglut2, or both Vgat and Vglut2 is similar for sequencing (Seq) and FISH. Astro, astrocytes; Endo, endothelial cells; EOC, extraosseous osteopontin-expressing cells; Mch, melanin-concentrating hormone; MG, microglia; Olig, oligodendrocytes; OPC, oligodendrocyte precursor cells; Orx, orexin/hypocretin; Peri, pericytes; VSM, vascular smooth muscle.

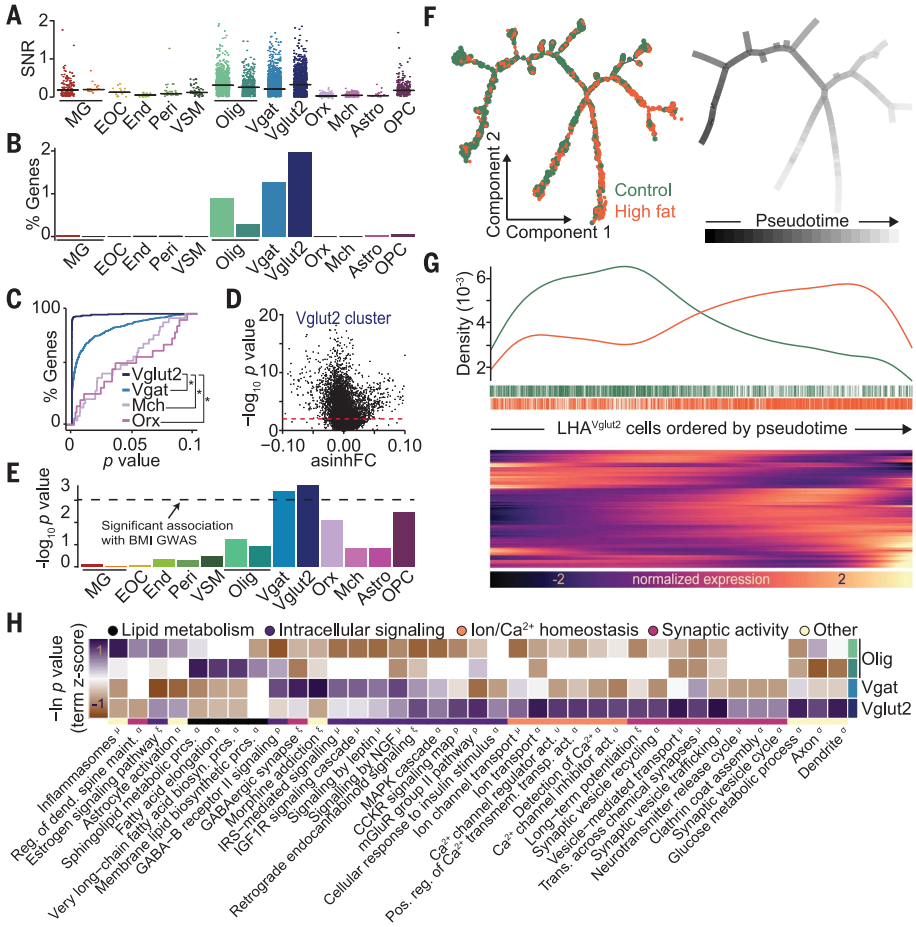

Fig. 2. HFD alters the transcriptional profile of LHA^{Vglut2} neurons. (**A**) Signal-to-noise ratio (SNR) of significantly altered genes ($P \leq 0.001$) within each cluster. Outliers with SNR > 2 are clipped for display. (**B**) Percentages of total genes significantly altered ($P \leq 0.0001$) in ≥50% of cells per cluster. (**C**) Cumulative distribution of P values ($P \leq 0.1$) for differentially expressed genes (DEGs) within each neuronal cluster and detected in ≥50% of cells per cluster. *$P < 0.0001$. (**D**) P values for asinh fold change (FC) for all genes within the Vglut2 cluster. (**E**) Gene-level genetic association with human BMI across clusters. Dashed line, Bonferroni significance threshold. (**F**) Pseudotime trajectories across control and HFD cells. (**G**) HFD cells are enriched at later pseudotimes (top) and show distinctive gene expression patterns (bottom, abridged from fig. S4). (**H**) DEGs ($P \leq 0.001$) queried against multiple annotation databases revealing altered expression in activity-dynamic–associated functional classes (see methods in the supplementary materials). In (A) to (E) and (H), DEGs between HFD and control cells were identified within each cluster (see methods and data S1).

cell type (Fig. 2, fig. S4A, and data S1). However, glutamatergic neurons, expressing vesicular glutamate transporter type-2 [Vglut2 (*Slc17a6*); LHA^{Vglut2}] exhibited significant changes in the greatest proportion of genes (Fig. 2, A to D). Consistently, LHA^{Vglut2} neurons also contained the most significant gene-level genetic association with human body mass index (BMI) (Fig. 2E), suggesting that similar alterations within LHA^{Vglut2} neurons may contribute to human obesity. This agrees with previous reports in which diet alters hypothalamic neurons involved in energy balance (*14*, *15*).

We next used LHA^{Vglut2} cells to construct unsupervised learned trajectories in which cells are ordered according to their predicted degree of transcriptional change, referred to as pseudotime (*16*). LHA^{Vglut2} HFD cells showed a gradient in the degree of transcriptional change, with enrichment of these cells at later pseudotimes. We compared differential gene expression between the most-altered (late pseudotime) and least-altered (early pseudotime) HFD cells along the entire trajectory and observed significant changes in the expression of genes associated with neuronal activity (Fig. 2, F and G, fig. S4B, and data S2). Considering these findings, we statistically examined functional annotations in genes differentially expressed across all LHA^{Vglut2} cells and found that LHA^{Vglut2} cells exhibited significant alterations in annotations associated with neuronal activity, including ion homeostasis, synaptic activity, and intracellular signaling. These annotations were distinct from those observed in vesicular γ-aminobutyric acid transporter [Vgat (*Slc32a1*)]-expressing cells or oligodendrocytes (Fig. 2H and data S2) (*17*).

Because LHA^{Vglut2} neurons were particularly sensitive to the HFD, we sought to assess their natural activity dynamics during caloric reward consumption. We hypothesized that acute food deprivation influences LHA^{Vglut2} activity dynamics. We infused an adeno-associated viral construct encoding Cre-dependent GCaMP6 (AAVdj-DIO-GCaMP6m) into the LHA of Vglut2-Cre mice and then implanted a microendoscopic lens ~150 μm above the injection site, permitting optical access to LHA^{Vglut2} neurons (Fig. 3, A to D). In brain slices, deflections in the GCaMP signal reliably tracked LHA^{Vglut2} action potential frequency (fig. S5, A and B). Calcium dynamics were measured in vivo with two-photon microscopy (*18*) as head-fixed mice consumed randomly delivered sucrose rewards. Individual LHA^{Vglut2} neurons were excited after sucrose consumption. Response magnitude depended on the mouse's motivational state (Fig. 3, E to I, and fig. S5F). After prefeeding, when motivation for food was low, responses of the same LHA^{Vglut2} neurons were greater than those after a 24-hour fast. This difference was independent of differences in lick rate (fig. S5, C to E), suggesting that satiety modifies LHA^{Vglut2} reward encoding independently of specific motor output. The neural responses during sucrose consumption could thus be used to decode (*19*) the motivational state of each mouse (Fig. 3J). Fasting also reduced basal calcium dynamics (fig. S5, G to J). LHA^{Vglut2} neuron stimulation transiently suppressed consummatory licking in a frequency-dependent fashion and was aversive (figs. S6 and S7) (*8*, *10*). We next aimed to test whether obesity alters this negative feeding regulator.

We hypothesized that LHA^{Vglut2} neuron activity dynamics and reward-encoding properties are modified by a HFD. Mice from the above experiment were maintained on either a HFD or a control diet for 12 weeks (Fig. 4A). The HFD potentiated weight gain (Fig. 4B). Whereas LHA^{Vglut2} neurons from control mice maintained their responsivity to sucrose consumption, LHA^{Vglut2} neurons from HFD mice became progressively less responsive to sucrose consumption (Fig. 4, C to E) and less active at rest (fig. S8, A to C). Concordantly, neural decoding of diet was most effective at 12 weeks (Fig. 4F and fig. S8E). A subset of neurons was tracked throughout the experiment and showed similarly blunted sucrose responses after exposure to a HFD (Fig. 4, G and H, and fig. S8, E to J), confirming that

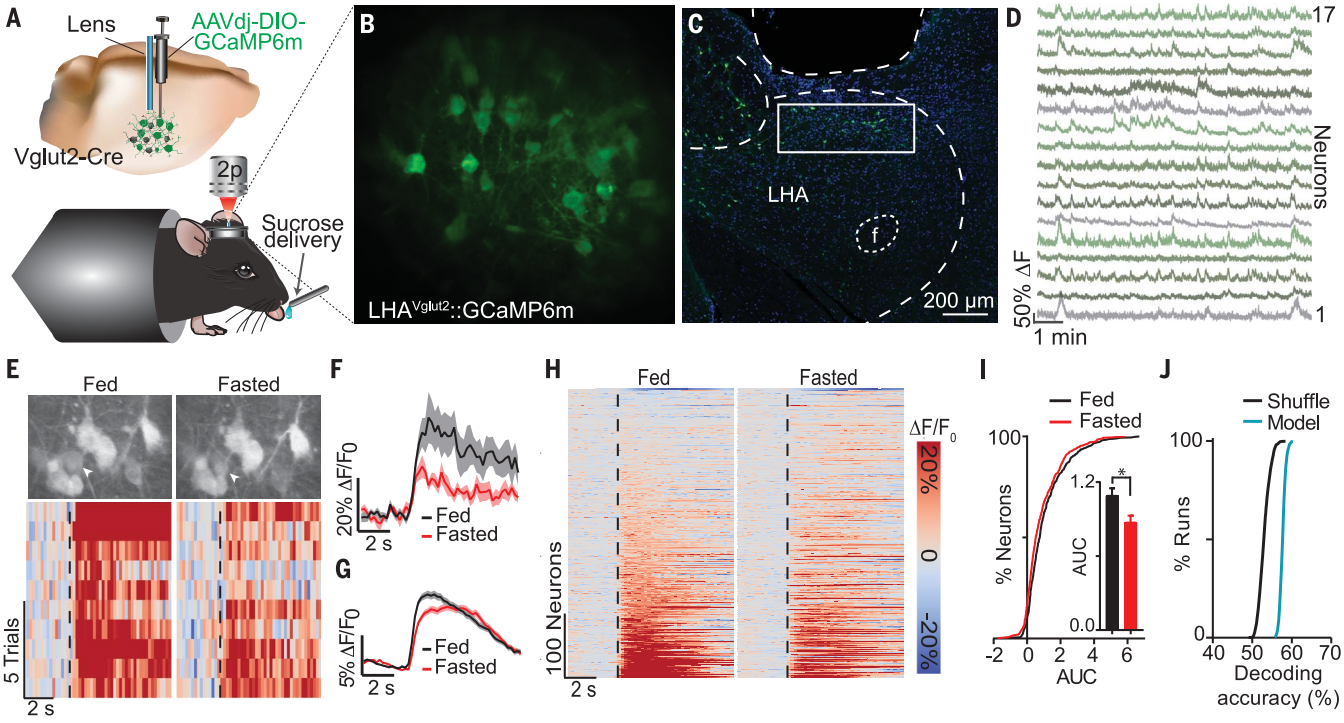

Fig. 3. LHA^{Vglut2} neurons encode satiety state. (**A**) Schematic of head-fixed two-photon imaging. (**B**) Example imaging plane (mean projection). (**C**) Confocal micrograph of lens position and GCaMP6m expression. f, fornix. (**D**) Extracted signals from a subset of neurons in (B). (**E**) Example neuron (arrow) whose response to sucrose was mediated by satiety. Data are aligned to sucrose consumption (dashed line). (**F**) Average response of neuron in (E). (**G**) Population average (452 neurons; 13 mice). (**H**) Responses from all neurons in the fasted and fed states. (**I**) Area under the curve (AUC) distributions (*P < 0.05). (**J**) Neural activity was used to decode the mouse's satiety state (P = 0.002). Values are means ± SEM.

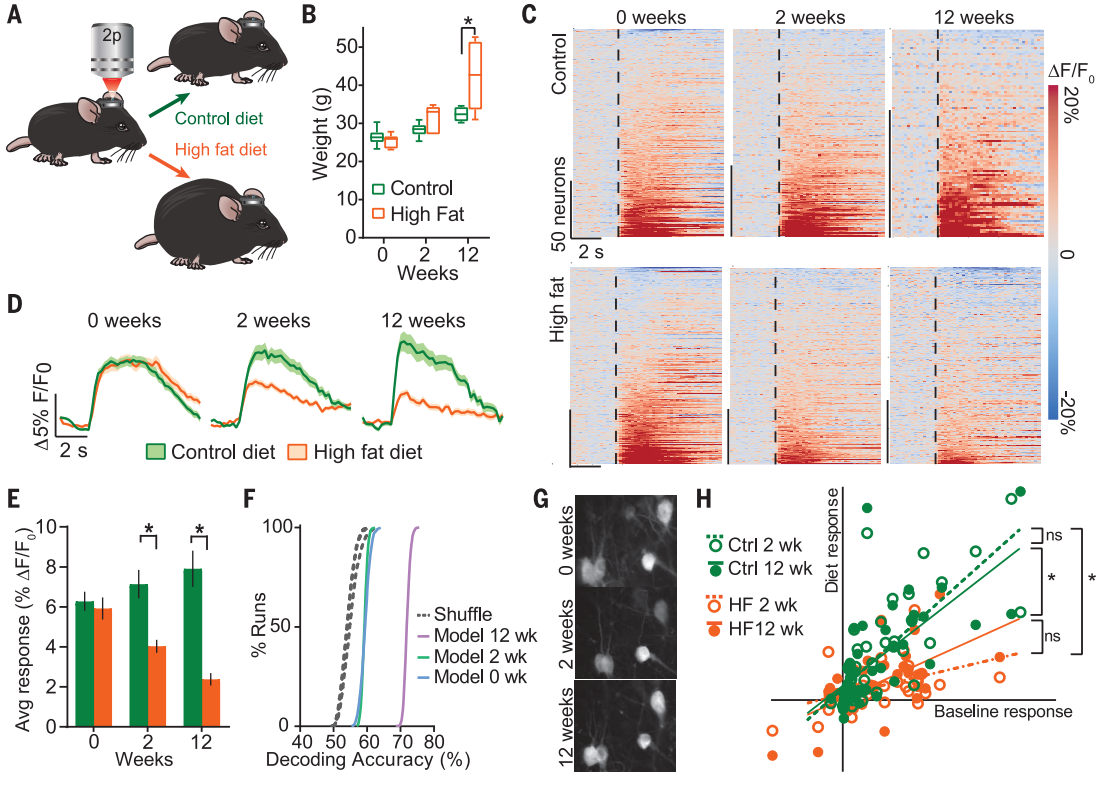

Fig. 4. Chronic HFD suppresses LHA^{Vglut2} activity. (**A**) Experimental design schematic. (**B**) Mouse weights (n = 7 in HFD group; n = 6 in control group). (**C**) Responses of all neurons to sucrose consumption. F, fluorescence; F_0, baseline fluorescence. (**D**) Average response of LHA^{Vglut2} neurons to sucrose consumption during obesity. For 0 weeks, 232 neurons (6 control mice), 220 neurons (7 HFD mice); for 2 weeks, 188 neurons (6 control mice), 231 neurons (7 HFD mice); for 12 weeks, 105 neurons (4 control mice), 201 neurons (7 HFD mice). (**E**) Mean sucrose response magnitude during diet exposure. Error bars indicate SEM. (**F**) Diet was decoded from sucrose responses. Decoding was most accurate at 12 weeks [P < 0.01 (12 weeks versus 0 and 2 weeks)]. (**G**) Example of neurons tracked during obesity (mean projections). (**H**) A subset of neurons was tracked throughout obesity (control: 44 cells, 4 mice; HFD: 33 cells, 4 mice). Sucrose response magnitudes at 2 and 12 weeks are plotted against the magnitude of the baseline (0 weeks) responses. *P < 0.05. ns, not significant.

individual LHA^{Vglut2} neurons alter their food reward encoding during obesity. Patch clamp electrophysiology revealed that reduced excitability underlies HFD-induced LHA^{Vglut2} suppression (fig. S9).

Until now, obesity's effects on the LHA have been unclear. We hypothesize that the excitatory LHA^{Vglut2} signal represents the activation of a brake on feeding to suppress further food intake. Here, we demonstrate that LHA^{Vglut2} neurons are sensitive to satiety state: when motivation for food is low, they are more excitable than when motivation is high. Chronic HFD modification within LHA^{Vglut2} cells ultimately hinders their neuronal activity, thereby weakening an endogenous attenuator of feeding to promote overeating and obesity.

Although this analysis focuses on glutamatergic neurons, this dataset provides a rich resource for identifying biologically meaningful transcriptional alterations across additional LHA neuronal, glial, and stromal cell types in response to a HFD. In addition to regulating consummatory behavior for food during obesity, LHA^{Vglut2} cells also contribute to aversion (fig. S7, M to O) (*8*, *20*–*22*), but it remains unclear whether these two populations are segregated. Whether LHA^{Vglut2} neuron alterations are normalized by returning to standard diet or if they are influenced by additional homeostatic challenges (e.g., dehydration) is unknown. Further understanding of the multifunctionality within this population could identify new therapeutic targets for eating disorders and obesity.

Note added in proof: A recent paper also characterized LHA heterogeneity using single-cell RNA sequencing (*23*).

REFERENCES AND NOTES

1. M. M. Finucane *et al*., *Lancet* **377**, 557–567 (2011).
2. P. G. Kopelman, *Nature* **404**, 635–643 (2000).
3. B. G. Hoebel, P. Teitelbaum, *Science* **135**, 375–377 (1962).
4. M. A. Rossi, G. D. Stuber, *Cell Metab.* **27**, 42–56 (2018).
5. R. A. Wise, *Science* **162**, 377–379 (1968).
6. D. L. Margules, J. Olds, *Science* **135**, 374–375 (1962).
7. B. K. Anand, S. Dua, K. Shoenberg, *J. Physiol.* **127**, 143–152 (1955).
8. J. H. Jennings, G. Rizzi, A. M. Stamatakis, R. L. Ung, G. D. Stuber, *Science* **341**, 1517–1521 (2013).
9. J. H. Jennings *et al*., *Cell* **160**, 516–527 (2015).
10. A. M. Stamatakis *et al*., *J. Neurosci.* **36**, 302–311 (2016).
11. E. H. Nieh *et al*., *Cell* **160**, 528–541 (2015).
12. E. Z. Macosko *et al*., *Cell* **161**, 1202–1214 (2015).
13. R. Satija, J. A. Farrell, D. Gennert, A. F. Schier, A. Regev, *Nat. Biotechnol.* **33**, 495–502 (2015).
14. F. E. Henry, K. Sugino, A. Tozer, T. Branco, S. M. Sternson, *eLife* **4**, e09800 (2015).
15. R. Chen, X. Wu, L. Jiang, Y. Zhang, *Cell Reports* **18**, 3227–3241 (2017).
16. C. Trapnell *et al*., *Nat. Biotechnol.* **32**, 381–386 (2014).
17. M. V. Kuleshov *et al*., *Nucleic Acids Res.* **44**, W90–W97 (2016).
18. J. A. McHenry *et al*., *Nat. Neurosci.* **20**, 449–458 (2017).
19. J. M. Otis *et al*., *Nature* **543**, 103–107 (2017).
20. E. H. Nieh *et al*., *Neuron* **90**, 1286–1298 (2016).
21. I. Lazaridis *et al*., *Mol. Psychiatry* 10.1038/s41380-019-0369-5 (2019).
22. M. Trusel *et al*., *Neuron* **102**, 120–127.e4 (2019).
23. L. E. Mickelsen *et al*., *Nat. Neurosci.* **22**, 642–656 (2019).

ACKNOWLEDGMENTS

We thank L. Eckman and R. Ying for assistance with mouse breeding, V. Namboodiri for analysis code, and Stuber lab members and C. Trapnell for helpful discussions. We thank K. Deisseroth (Stanford University) and the GENIE project at Janelia Research Campus for viral constructs. **Funding:** This study was funded by grants from the National Institutes of Health [NIDDK DK112564 (M.A.R.), NIMH MH093315 and MH115165 (J.A.M.), NS007431 (M.L.B.), NIDA DA041184 (J.M.O.) and DA038168 and DA032750 (G.D.S.)], the Foundation of Hope (J.A.M. and G.D.S.), the Brain and Behavior Research Foundation (NARSAD Young Investigator awards to J.A.M., J.M.O., and M.A.R.), UNC Neuroscience Center Microscopy Core (P30 NS045892), the Swedish Research Council (VR Dnr 538-2013-8864 to C.M.B.), and the Swiss National Science Foundation (J.B.). This study represents independent research funded in part by the National Institute for Health Research (NIHR) Biomedical Research Centre at South London and Maudsley NHS Foundation Trust and King's College London. The views expressed are those of the author(s) and not necessarily those of the NHS, the NIHR, or the Department of Health. High-performance computing facilities were funded with capital equipment grants from the GSTT Charity (TR130505) and Maudsley Charity (980). This study was completed as part of approved UK Biobank study application 27546 to G.B. **Author contributions:** M.A.R., M.L.B., and G.D.S. conceived and designed experiments. M.A.R. performed surgery, imaging, and analysis. M.L.B. performed sequencing. M.A.R. and M.L.B. analyzed sequencing data. M.A.R., J.A.M., and O.K. performed in situ hybridization. M.A.R. and J.M.O. performed slice electrophysiology. M.A.R., H.E.v.d.M., and W.G. performed optogenetic testing. M.A.R., M.L.B., and G.D.S. wrote the manuscript with input from all authors. J.B., C.H., P.F.S., C.M.B., and G.B. performed the genome-wide association analysis. **Competing interests:** G.B. has received grant funding from and served as a consultant to Eli Lilly and has received honoraria from Illumina. C.M.B. is a grant recipient from and has served on advisory boards for Shire. She receives royalties from Pearson and Walker. All interests are unrelated to this work. **Data and materials availability:** Datasets are available on NCBI Gene Expression Omnibus (accession no. GSE130597).

SUPPLEMENTARY MATERIALS

science.sciencemag.org/content/364/6447/1271/suppl/DC1
Materials and Methods
Figs. S1 to S9
Table S1
References (*24*–*41*)
Data S1 and S2

26 February 2019; accepted 10 May 2019
10.1126/science.aax1184